PHYSICAL REVIEW APPLIED **14,** 064046 (2020)

Featured in Physics

Information Carried by Electromagnetic Radiation Launched from Accelerated Polarization Currents

John Singleton,[1,*] Andrea C. Schmidt,[1,†] Connor Bailey,[1] James Wigger,[1] and Frank Krawczyk[2]

[1] *National High Magnetic Field Laboratory, MPA-MAGLAB, MS-E536, Los Alamos National Laboratory, Los Alamos, New Mexico 87545, USA*
[2] *Accelerators and Electrodynamics, AOT-AE, MS-H851, Los Alamos National Laboratory, Los Alamos, New Mexico 87545, USA*

(Received 3 June 2020; revised 29 September 2020; accepted 9 November 2020; published 15 December 2020)

We show experimentally that a continuous, linear, dielectric antenna in which a superluminal polarization-current distribution accelerates can be used to transmit a broadband signal that is reproduced in a comprehensible form at a chosen target distance and angle. The requirement for this exact correspondence between broadcast and received signals is that each moving point in the polarization-current distribution approaches the target at the speed of light at all times during its transit along the antenna. This results in a one-to-one correspondence between the time at which each point on the moving polarization current enters the antenna and the time at which *all* of the radiation emitted by this particular point during its transit through the antenna arrives simultaneously at the target. This has the effect of reproducing the desired time dependence of the original broadcast signal. For other observer-detector positions, the time dependence of the signal is scrambled, due to the nontrivial relationship between emission (retarded) time and reception time. This technique represents a contrast to conventional radio transmission methods; in most examples of the latter, signals are broadcast with little or no directivity, selectivity of reception being achieved through the use of narrow frequency bands. In place of this, the current paper uses a spread of frequencies to transmit information to a particular location; the signal is weaker and has a scrambled time dependence elsewhere. We point out the possible relevance of this mechanism to 5G neighborhood networks and pulsar astronomy.

DOI: 10.1103/PhysRevApplied.14.064046

I. INTRODUCTION

Though the subject has been studied for over a century [1–3], in the past 20 years there has been renewed interest in the emission of radiation by polarization currents that travel faster than the speed of light *in vacuo* [4–10]. Such polarization currents may be produced by photoemission from a surface excited by an obliquely incident, high-power laser pulse [4–8]. Alternatively, in *polarization-current antennas*, they are excited by the application of carefully timed voltages to multiple electrodes on either side of a slab of a dielectric such as alumina [9–15]. To illustrate these emission mechanisims, we write the third and fourth Maxwell equations [16–19] in the following form:

$$\nabla \times \mathbf{E} + \frac{\partial \mathbf{B}}{\partial t} = 0, \tag{1}$$

$$\nabla \times \mathbf{H} - \varepsilon_0 \frac{\partial \mathbf{E}}{\partial t} = \mathbf{J}_{\text{free}} + \frac{\partial \mathbf{P}}{\partial t}. \tag{2}$$

Here **E** is the electric field, **H** is the magnetic field, **B** [$= \mu_0(\mathbf{H} + \mathbf{M})$] is the magnetic flux density, **M** is the magnetization, **P** is the polarization (i.e., the dipole moment per unit volume), and $\mathbf{J}_{\text{free}}$ is a current density of mobile charges. The terms on the left-hand side of both expressions are coupled equations that describe the propagation of electromagnetic waves [16,18], whereas the terms on the right-hand side of Eq. (2) may be regarded as *source terms* [17,19]. The current density $\mathbf{J}_{\text{free}}$ of free charges (usually electrons) is used to generate electromagnetic radiation in almost all conventional applications such as phased arrays and other antennas [17], synchrotrons [20], light bulbs [18] etc. By contrast, the emission mechanisms mentioned above employ the polarization current density, $\partial \mathbf{P}/\partial t$, as their source term [9–15].

In this paper, we use an experiment to study the information conveyed in the signals broadcast by such polarization currents when they are accelerated. We find that a time-dependent amplitude modulation is reproduced exactly in the received signal only when the detecting antenna is close to a particular set of points, the position of which is related to details of the acceleration. At other points, the signal is scrambled. The result has implications for

---

[*] jsingle@lanl.gov
[†] aschmidt@lanl.gov

communication applications and for astronomical observations of objects such as pulsars.

The paper is organized as follows. Section II gives a brief introduction to the type of polarization-current antenna used in this work, and how the polarization current within it is animated and accelerated; as the antennas may not be familiar to the general reader, additional detail is given in the Supplemental Material [21]. Section III gives an account of the acceleration scheme for transmitting information to particular locations. Sections IV and V describe an experimental proof of concept of the effect carried out within a 6.5-m rf anechoic chamber. Finally, Sec. VI discusses the implications of this observation for communications and astronomy.

II. POLARIZATION-CURRENT ANTENNAS

In both dielectric resonator antennas (DRAs) [22] and polarization-current antennas (PCAs) dielectrics play a major role in the emission mechanisms. However, the two antenna types function in completely different ways; DRAs essentially use the dielectric to boost the effective size (and hence the efficiency) of a small antenna [22], whereas in PCAs, the dielectric hosts a moving, volume-distributed polarization current [9–15]. Consequently, PCAs usually consist of a continuous strip of a dielectric such as alumina with electrodes on either side [Fig. 1(a)]. Each electrode pair and the dielectric in between is referred to as an *element*; the elements are supplied independently with a voltage difference, $V = V_U - V_L$, where U and L refer to upper and lower electrodes. This produces polarization $\mathbf{P}$ in the dielectric. By changing $V_U - V_L$ on a series of elements, the polarized region is moved [Figs. 1(a) and 1(b)]; owing to the time dependence imparted by movement, a polarization current, $\partial\mathbf{P}/\partial t$ is produced, and will, under the correct conditions, emit electromagnetic radiation [2,3,9–15].

PCAs are usually run by moving a continuous polarization current along the dielectric [12–15]. This is accomplished by applying phase-shifted time-dependent signals to the elements [21]. A simple example is given in Fig. 1(c), where the upper (green) trace shows $[V_U - V_L]_j = \sin[\omega(t - j\,\Delta t)]$ versus j, where j labels the antenna element, ω is an angular frequency, t is time and Δt is a time increment, at $t = 0$. The lower (red) trace shows $[V_U - V_L]_j$ at a later time; the effect of the time increments is to move the "voltage wave" and hence the induced polarization at a speed $v = a/\Delta t$, where a is the distance between element centers. Acceleration is introduced by varying Δt along the antenna's length. Further details and typical emission properties are given in the Supplemental Material [21].

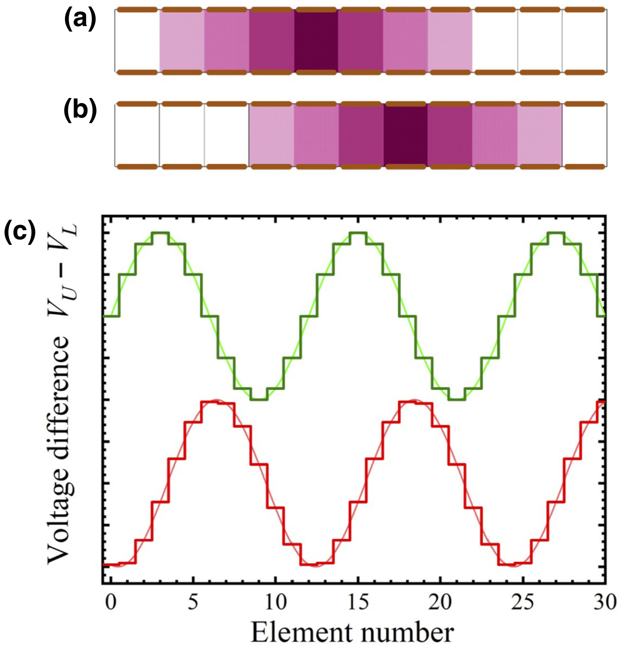

FIG. 1. (a) Polarization-current antennas (PCAs) consist of a continuous series of elements made of a dielectric (white) sandwiched between pairs of electrodes (orange). The dielectric is polarized by applying a voltage difference $V_U - V_L$ between upper (U) and lower (L) electrodes; this is shown schematically for seven elements, the shading density representing the polarization strength. (b) The $V_U - V_L$ shown in (a) are applied to elements two further to the right, moving the polarized region. (c) The upper (green) trace shows $[V_U - V_L]_j = \sin[\omega(t - j\,\Delta t)]$ versus j, where j labels the antenna element, ω is an angular frequency, t is time, and Δt is a time increment, at $t = 0$. The lower (red) trace (offset vertically for clarity) shows $[V_U - V_L]_j$ at $t = \frac{103}{180}(2\pi/\omega)$; the effect of the timing differences is to move the "voltage wave" (and the induced polarization) along. In practice, fringing effects round off the stepped voltages, leading to a smoother waveform (fine liines).

The practical antenna used in the experiments below is shown in Fig. 2(a); it has 32 elements spanning a total length of 0.64 m, and the dielectric is alumina ($\varepsilon_r \approx 10$). The elements are fed via a 32-way splitter and 32 mechanical delay lines [Fig. 2(b)] which are adjusted to produce time differences Δt [14]. Note that in these antennas, the polarization current fills the entire dielectric; it is a continuously moving source of radiation that emits from an extended volume, rather than at a series of points or lines (as in a phased array). Despite the discrete nature of the electrodes, simulations of our antennas performed with off-the-shelf electromagnetic software packages such as Microwave Studio show that fringing fields of adjacent electrode pairs lead to a voltage phase that varies slightly under the electrode [23]; i.e., the phase is more smoothly varying along the length of the antenna than the discrete arrangement of electrodes suggests [21,24]. This is represented by the smoother curves in Fig. 1(c).

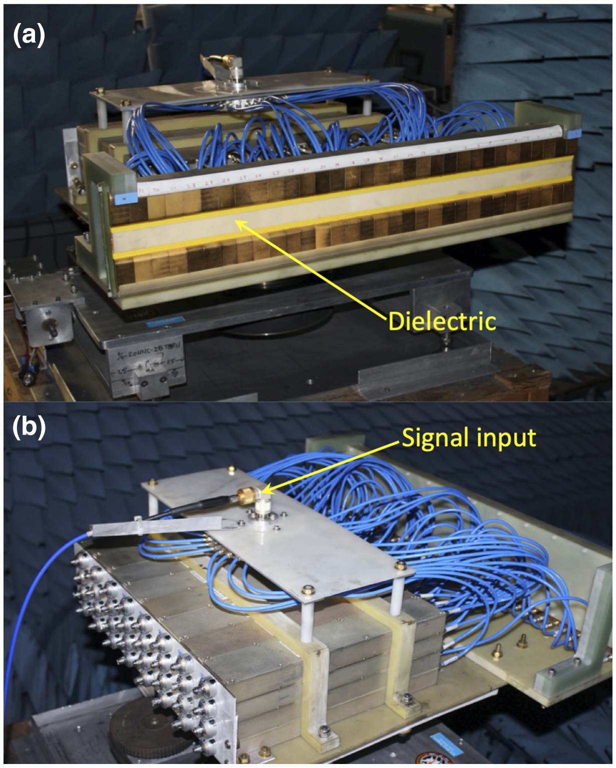

FIG. 2. (a) Front view of the passive antenna used in the demonstration experiment mounted on its turntable in the anechoic chamber. It has 32 elements spanning a total length of 0.64 m. The label indicates the cream-colored dielectric (alumina) that hosts the volume-distributed moving polarization current responsible for the emission of radio waves from the antenna. (b) Rear view of the antenna showing the 32-way splitter feeding 32 independent ATM P1214 mechanical phase shifters. The dials for adjusting the phase are visible on the lower left of the picture. The signal input on the top of the 32-way splitter is labeled.

III. CONCEPT: ACCELERATION AND FOCUSING

We now consider an antenna containing a "wavepacket" of polarization current that has finite extent in both space and time; it moves on a linear trajectory and accelerates. Figure 3(a) shows a plan view of the antenna's dielectric of length $2y_0$ with its center at $(0,0,0)$ lying along the Cartesian y axis. As in the experimental antennas [13–15] [Fig. 2(a)] the dielectric has rectangular cross section; its depth $2x_0$ (extent in the x direction) and height $2z_0$ (extent in the z direction) are symmetrical about the y axis; both x_0 and z_0 are $\ll y_0$.

A target is chosen in the (x,y) plane at a distance R_0; the angle Ψ_0 "off boresight" describes the target's azimuthal position. As everything of interest lies in the (x,y) $(z=0)$ plane, for convenience we drop the Cartesian z coordinate for the time being. Thus, the target is at $(X_0,-Y_0)$, where

$$X_0 = R_0\cos\Psi_0 \quad \text{and} \quad |Y_0| = R_0\sin\Psi_0. \tag{3}$$

Consider a point in the polarization current that is moving through the dielectic along the y axis; the instantaneous distance r between the point at $(0,y)$ and the target at (X_0,Y_0) is given by

$$r^2 = X_0^2 + (Y_0+y)^2. \tag{4}$$

The point is made to move in such a way that the component of its velocity towards the target is always c, the speed of light in the surrounding medium (assumed to be vacuum), that is $(dr/dt) = -c$, where t is the time. Differentiating Eq. (4) with respect to t, inserting the above value for (dr/dt) and rearranging, we obtain the point's velocity along y:

$$\frac{dy}{dt} = -c\frac{\left[X_0^2+(Y_0+y)^2\right]^{1/2}}{Y_0+y}. \tag{5}$$

Integrating Eq. (5), and assuming that the point commences its journey along the antenna at $y=y_0$ and time $t=0$, we obtain a relationship between the point's position y and time t:

$$t = \frac{1}{c}\left\{[X_0^2+(Y_0+y_0)^2]^{1/2} - [X_0^2+(Y_0+y)^2]^{1/2}\right\}. \tag{6}$$

We now consider a detector placed at a general point P with coordinates $(X,-Y)$ in the (x,y) plane. The radiation emitted by the point as it travels along the antenna will reach P at a time t_P given by

$$\begin{aligned} t_p &= t + \frac{1}{c}[X^2+(Y+y)^2]^{1/2} \\ &= \frac{1}{c}\Big\{[X_0^2+(Y_0+y_0)^2]^{1/2} - [X_0^2+(Y_0+y)^2]^{1/2} \\ &\quad + [X^2+(Y+y)^2]^{1/2}\Big\}. \end{aligned} \tag{7}$$

It should be obvious that if, *and only if*, $X=X_0$ and $Y=Y_0$, then $t_P=$ a constant. For all other choices of detector position, t_P is a function of y and therefore of t.

This situation is illustrated in the first two columns of Fig. 4. The intended target $(X_0,-Y_0)$ is at $R_0=5$ m from the antenna center and at $\Phi_0=15°$ [Fig. 4, row (a), left column]; if the detector P is placed *exactly* at this position, then $t_P=$ constant [row (a), center column]. The constant here is the transit time of light from $y=y_0$, the place at which the point source enters the antenna at $t=0$, to the target; subsequently the accelerated motion of the point source along the antenna exactly compensates for the changing point-to-target distance. If, on the other hand, the detector position P is not at $(X_0,-Y_0)$ [Fig. 4, rows (b) and (c)], then t_P is a function of t.

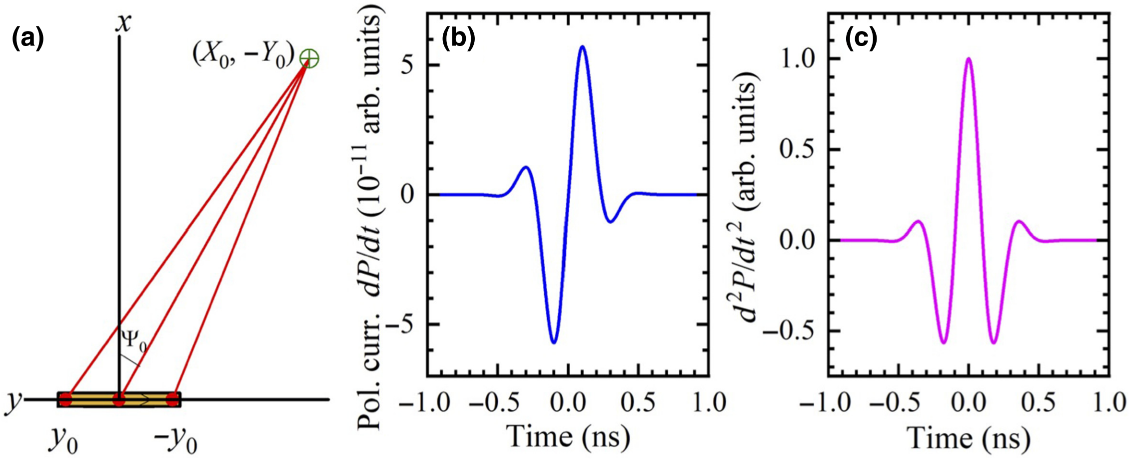

FIG. 3. (a) Experimental concept. An element of polarization current (red) moves along the dielectric antenna (dark yellow shading) such that the component of its velocity in the direction of the target [green cross at $(X_0, -Y_0)$] is always c, the speed of light. The center of the antenna is at $(0, 0)$. (b) Notional time dependence of the polarization current dP/dt sent along the antenna. (c) Derivative of the curve shown in (b) with respect to time t. The “arbitrary units” in (c) are equivalent to those in (b), the large scaling occurring because of the fast time dependences.

Next, rather than a single point, we consider the movement of the whole time-dependent polarization-current waveform along the antenna [25]. The imposed motion is such that *each* point within the waveform is accelerated as described above; i.e., as it traverses the antenna, such a point always has a velocity component c in the direction of the target. Referring to the discussion of Eq. (7) above, all radiation emitted by this point as it moves along the antenna will arrive at the target at a time given by $t_P =$ (time that point enters the antenna at $y = y_0$) + (transit time of light from $y = y_0$ to the target). Therefore, there is a one-to-one correspondence between the time at which each point on the moving waveform enters the antenna and the arrival time at the target of the radiation emitted by this particular point as it traverses the antenna.

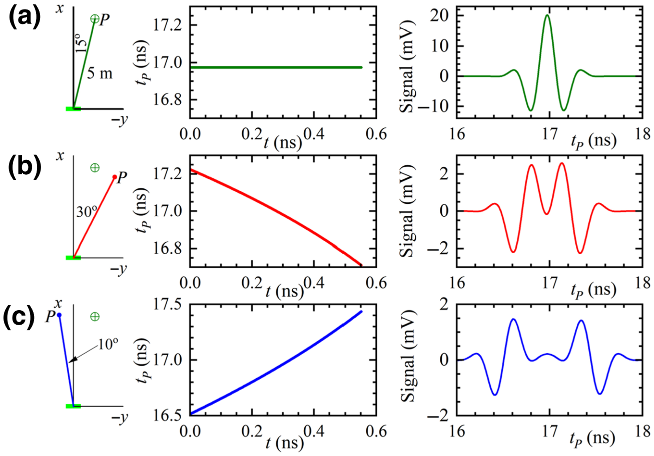

FIG. 4. Each row shows the effect of moving the detector to positions P 5 m from the antenna center (light green). In each row, the left panel gives position P, the center shows the arrival time t_P of radiation emitted at time t by a point accelerating along the antenna, and the right is the signal detected due to the polarization current of Fig. 3(b) being accelerated along the antenna. In all cases, the target (green cross) is 5 m from the antenna center at an angle of 15° to the x axis. Row (a): detector at target position. Row (b): detector placed on a line making an angle of 30° with the x axis. Row (c): detector placed 10° to the other side of the x axis.

To show how this affects the received radiation, we send the waveform shown in Fig. 3(b) along the antenna with the constraint that each point on the waveform obeys the acceleration scheme described by Eqs. (3) and (6); as before $\Phi_0 = 15^\circ$ and $R_0 = 5.0$ m. The resulting signals (proportional to the E field) for the detector positions given in the first column of Fig. 4 are shown in the third column of the same figure; the Supplemental Material describes how such calculations are carried out [21,24]. At the target angle and distance [Fig. 4, row (a)], the detected signal reproduces the shape of the time derivative of the polarization-current waveform [Fig. 3(c)] exactly. Away from the target position [Fig. 4, rows (b) and (c)], the detected signal is much smaller and has altered frequency content and shape.

First, why is the time derivative of the polarization current reproduced? The calculations in the Supplemental Material show that [21,24] the magnetic vector potential $\mathbf{A}$ resulting from each volume element of the antenna is proportional to the polarization current within that element [Supplemental Material, Eq. (8) [21]]. The corresponding E field is proportional to the derivative of $\mathbf{A}$ with respect to time [18]. Therefore, it is the *electric field* launched from the antenna that is reproduced at, and only at, the target point.

The idea is illustrated in more detail in Fig. 5; (a) shows the launched E field [$\propto (d^2P/dt^2)$] at three different times indicated by different colors during its transit through the antenna. Figure 5(b) shows the corresponding detected E field at the target point. The colored lines linking the curves in Figs. 5(a) and 5(b) illustrate the principle that radiation from a particular point on the traveling waveform *always arrives at the same time at the target*. Thus, features in the launched E field are *reinforced* at the target in the correct time sequence. In other words, the time dependence of the emission of the whole waveform is reproduced at the target [compare Figs. 3(c) and 4(a)] whereas elsewhere, it is scrambled [Figs. 4(b) and 4(c)].

Figure 5(c) illustrates the same principle using Huyghens wavelets. The colored dots represent the positions of a particular point on the polarization-current waveform at different times during its transit of the antenna; semicircles of the same color represent the corresponding emitted Huyghens wavelets, arriving at the target (orange diamond) simultaneously. At other locations, the Huyghens wavelets arrive at different times, so that the signal becomes scrambled.

For the experimental demonstration below, we need to describe a polarization-current waveform the possesses the required motion for the above focusing effects. To do this, we write [25]

$$\frac{\partial \mathbf{P}}{\partial t} = \mathbf{f}(y,t) = \mathbf{f}[t - p(y)], \tag{8}$$

where $\mathbf{f}$ is a vector function of time t and the function $p(y)$. Constant phase points are represented by $t - p(y) =$ constant; differentiating this with respect to t results in

$$1 = \frac{dp}{dt} = \frac{dp}{dy}\frac{dy}{dt}. \tag{9}$$

Substituting from Eq. (5) and integrating, we obtain

$$p(y) = -\frac{\left[X_0^2 + (Y_0 + y)^2\right]^{1/2}}{c}. \tag{10}$$

Equations (8) and (10) describe the required extended polarization-current waveform, all of the points within which approach the target at a speed of c.

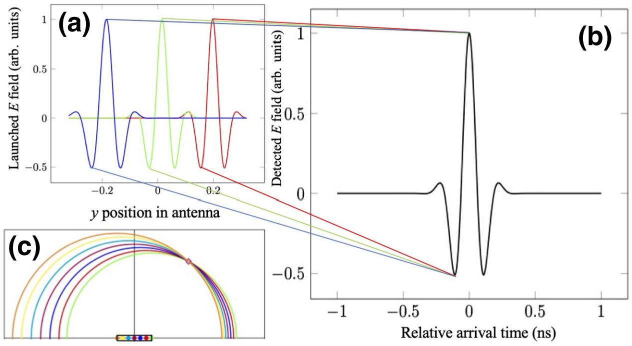

FIG. 5. (a) Launched E field [$\propto (d^2P/dt^2)$], corresponding to a polarization current similar to that in Fig. 3(b), at three different times (denoted by red, green, and blue curves) during its transit along the antenna; note that the waveform "stretches out" due to the acceleration parameterized by Eqs. (3) and (6). (b) The corresponding detected E field at the target point; colored lines linking (a),(b) show schematically the principle that radiation from a particular point on the traveling waveform arrives at the same time at the target. This is because the acceleration compensates exactly for the different distances between source point and detection locations [see Eq. (7) *et seq.*]. Hence, features in the launched E field are reinforced in the correct time sequence in the detected signal. (c) The same principle is illustrated using Huyghens wavelets; colored dots in the antenna (dielectric outlined by black lines) represent the positions of a particular point on waveform (a) at different times during its transit of the antenna; semicircles of the same color show corresponding emittted Huyghens wavelets arriving at the focus point (orange diamond) simultaneously.

Finally, note that we have only treated a time-domain focus in the (x,y) plane. In fact the criterion for focusing—that points in the polarization-current distribution approach the observer-detector at the speed of light along their entire path though the antenna—is fulfilled on a *semicircle* of points around the antenna (our antennas are designed not to emit from their rear surfaces [14]) that extends in the y and z directions, with a radius $(y^2 + z^2)^{1/2} = Y_0$. However, in a proof-of-concept demonstration experiment, moving the observer-detector away from $z = 0$ complicates matters, as the radiation's E field is no longer vertically polarized; there is an additional component polarized parallel to y (this may be deduced from the calculations in the Supplemental Material [21]; for more details see Chapter 7 of Ref. [24]). In the next implementation of this concept, the single antenna discussed in the present paper is replaced by an array of linear antennas configured to allow full three-dimensional (x,y,z) control of the information focus point, along with minimization of the parasitic y polarization of the E field [26].

IV. EXPERIMENTAL DEMONSTRATION

The antenna shown in Fig. 2 is used for the experimental demonstration. It is mounted on a powered turntable (vertical rotation axis) with an azimuthal angular precision of ±0.1°. A Schwarzbeck-Mess calibrated dipole at the same vertical height is used to receive the vertically polarized transmitted radiation; this is mounted on a TDK plastic tripod on rails that allows it to be moved to different distances without changing the height or angular alignment of the equipment. The entire system is in a $5.8 \times 3.6 \times 3.6$ m^3 metal anechoic chamber completely lined with ETS-Lindgren EHP-12PCL pyramidal absorber tiles.

Signals received by the dipole are sent either to a Hewlett-Packard HP8595E spectrum analyzer to monitor power at a chosen frequency, or to a Mini-Circuits TVA-82-213A broadband amplifier that allows the time-dependent voltage to be viewed and/or digitized using a Tektronix TDS7404 digital oscilloscope. Care is taken to ensure that the cables used are shielded from the radiation within the anechoic chamber and that secondary-path signals are approximately 60 dB less than direct radiation from antenna to dipole.

The description in Sec. III is framed in terms of a traveling wavepacket. However, detecting a single pulse, especially if it contains a spread of frequencies, presents technical difficulties in a facility where only low power levels are permitted. Instead, we choose to transmit and detect what is in effect a train of wavepackets. This forms a continuous broadband signal with a distinctive shape, based on a mixture of harmonics of 0.90 GHz and synthesized by mixing outputs from phase-locked TTi TGR6000 and Agilent N9318 function generators. The synthesized signal is sent to a Mini-Circuits TVA-82-213A amplifier, the output of which drives a 32-way splitter feeding 32 independent ATM P1214 mechanical phase shifters [Fig. 2(b)]. The latter are used to set the time delays of the signals sent to each antenna element, reproducing the above acceleration scheme. To keep the "information focus" well within the anechoic chamber, $X_0 = 3.03$ m and $Y_0 = 0.64$ m are chosen, yielding target distance $R_0 = 3.09$ m and azimuthal angle $\Phi_0 = 11.9^\circ$.

The time dependence of the broadcast waveform is recorded by placing the receiver dipole 10 mm in front of the 16th element of the antenna and observing the signal on the oscilloscope. As long as the shortest emitted wavelength is much larger than the distance from the dielectric to the detector, the calculations described in the Supplemental Material [21] can be used to show that the E field thus detected by the dipole is, to a good approximation, $\propto \partial^2\mathbf{P}/\partial t^2$, where $\mathbf{P}$ is the polarization passing the point in the dielectric closest to the detector antenna. Hence, an analog of Fig. 3(c) for the experimental wavetrain is captured; moreover, any frequency-dependent artefacts are the same in the measurements of the broadcast and received signals, making a comparison analogous to that between Fig. 3(b) and the third column of Fig. 4 simpler.

The waveform used for the experiments is selected by adjusting the outputs of the two signal generators and is shown in Fig. 6(a). It is chosen because (i) it has a distinctive time-dependent shape (e.g., the double peak followed by two differing minima, one relatively broad) and (ii) an easily recognized "triangular" Fourier spectrum [Fig. 6(b)]. These traits aid in the rapid location of ranges of distance and azimuthal angle over which the broadcast signal is reproduced.

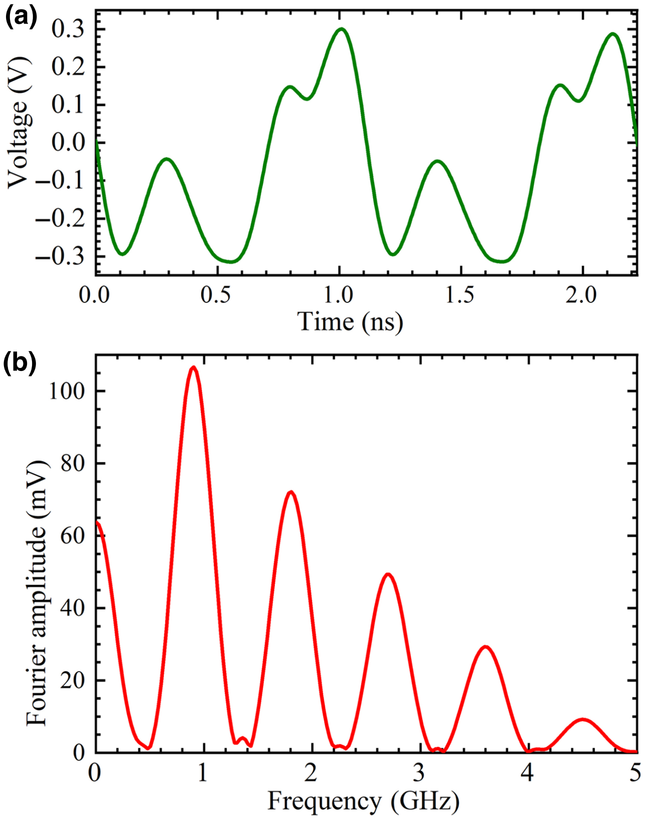

FIG. 6. (a) Voltage measured by placing the dipole receiver 10 mm in front of the 16th antenna element as a function of time; in effect, this is the desired transmitted signal. (b) Fourier transform of the waveform in (a). Note the distinctive "triangular" pattern of harmonics of 0.9 GHz.

V. RESULTS

Preliminary surveys are carried out by sweeping the transmitter azimuthal angle at closely spaced distances around the expected R_0 whilst carefully observing the received signal on the oscilloscope or spectrum analyzer. Slight phase-setting errors result in actual target coordinates $R_0 \approx 3.00$ m and $\Phi_0 \approx 11.6^\circ$ (cf. planned values of 3.09 m and 11.9°).

Once this "focus" is established, the transmitter-to-receiver distance is fixed at 3.0 m and the oscilloscope trace of the received signal recorded for several fixed azimuthal angles spaced by approximately 1°. The results of this procedure are shown in Fig. 7. On comparing with Fig. 6(a), it is clear that the broadcast signal (double peak, narrower then wider minimum) is only reproduced faithfully at an azimuthal angle of 11.6° (orange, thicker curve). The time-dependent signals for angles 12.8° and 10.5° show distinct differences from the broadcast waveform; one only has to move a few more degrees away from Ψ_0 and any resemblance to the broadcast signal is lost.

This picture is confirmed by Fourier transforms of the oscilloscope data [Fig. 8(a)]. At an angle of 11.6° (red

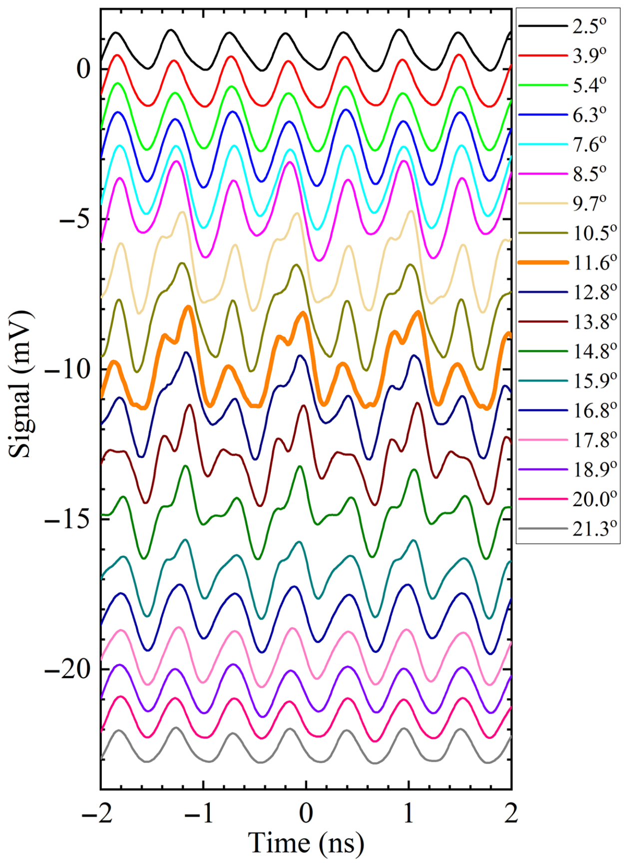

FIG. 7. Time dependence of the signal received by the detector dipole for an antenna-to-detector distance of 3.0 m and for the azimuthal angles shown in the key. The shape of the transmitted waveform [Fig. 6(a)] is only reproduced close to the "target" angle of 11.6° (orange trace). Experimental traces are offset vertically for clarity.

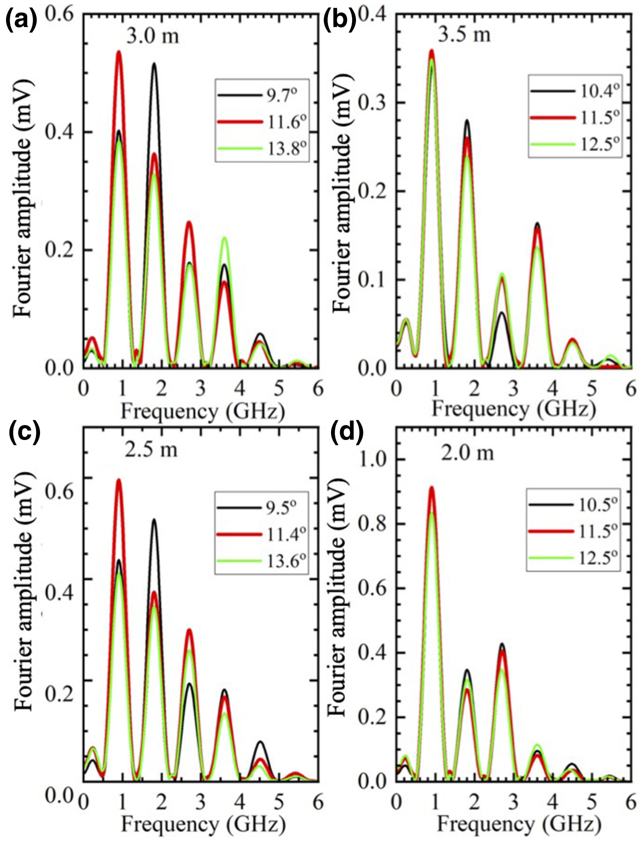

FIG. 8. Fourier transforms of the detector signal for azimuthal angles (shown in key) on either side of (green and black) and close to or at the target angle of 11.6° (red) and at different antenna-to-detector distances: (a) 3.0 m, (b) 3.5 m, (c) 2.5 m, and (d) 2.0 m.

trace), the expected "triangular" Fourier spectrum [cf. Fig. 6(b)] is produced. On moving approximately ±2° away, the relative amplitudes of the harmonics of 0.9 GHz change quite dramatically, showing that the frequency content present in the broadcast signal is being scrambled.

Measurements are then repeated at fixed transmitter-to-receiver distances either side of the target distance of $R_0 = 3.0$ m [Figs. 8(b)–8(d)]. Even azimuthal angles close to the target value (red traces) fail to yield the broadcast "triangular" Fourier spectrum [compare with Figs. 8(a), 6(b)], showing that the frequency content of the original broadcast signal is only reproduced when the distance *and* the azimuthal angle are close to the target values. Fourier transforms taken over wider angular ranges are given in the contour plots of Fig. 9, showing that the "triangular" Fourier spectrum is not recovered as one moves farther from the target angle. Figure 10 shows the effect on the time dependence of the received signal caused by keeping the azimuthal angle close to $\Phi_0 = 11.6°$ and varying the transmitter-to-receiver distance. Comparing Fig. 10 with Fig. 6(a), it is clear that the broadcast signal's time dependence (double peak, narrower and then wider minimum) is only reproduced faithfully at distances close to the target value of 3.0 m (orange, thicker curve).

VI. DISCUSSION

The data displayed in Figs. 6 to 10 show that a continuous, linear, dielectric antenna in which a superluminal polarization-current distribution accelerates can be used to transmit a broadband signal that is reproduced in a comprehensible form at a chosen target distance and angle; as noted in the final paragraph of Sec. III, effectively this signal is distributed onto a half circle [24] in the current implementation of the experiment [26]. The requirement for this exact correspondence between broadcast and received signals is that each point in the polarization-current distribution approaches the observer-detector at the speed of light at all times during its transit along the antenna. This results in all of the radiation emitted

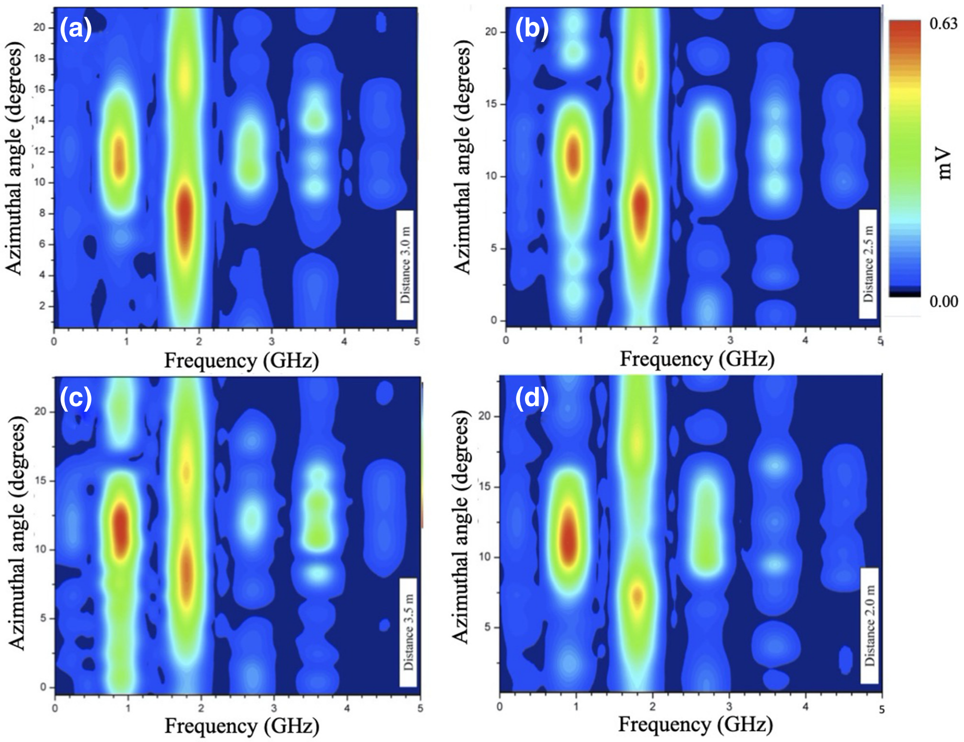

FIG. 9. Fourier transforms of the detector signal plotted as contour plots versus frequency and azimuthal angle for different antenna-to-detector distances: (a) 3.0 m, (b) 2.5 m, (c) 3.5 m, and (d) 2.0 m.

from this point as it traverses the antenna reaching the observer-detector at the same time [Fig. 4(a)]. For other observer-detector positions, the time dependence of the signal is scrambled, due to the nontrivial relationship between emission time and reception time [Figs. 4(b) and 4(c)].

The primary role of the current paper is to introduce the above effect and to demonstrate it experimentally. However, it is interesting to suggest how a PCA might be employed to transmit signals that contain information. Figure 11 depicts a simulation of a simple version of such a concept. The inset shows the time dependence of a wavepacket of launched E field that could function as a single "bit." Like the waveforms employed in Figs. 3 and 4, it consists of the convolution of a Gaussian and a cosine. The main part of the figure shows a calculation (using the techniques detailed in the Supplemental Material [21]) of the received signal due to the broadcast of two of these "bits," spaced in time by three periods of the cosine function. For ease of comparison, the antenna acceleration scheme [i.e., target angle (15°) and distance (5.0 m)] is the same as that employed in Fig. 4. At the target angle of 15°, the two "bits" can be distinguished clearly (labeled 1 and 2 in Fig. 11); as one moves the receiver away from the target angle by as little as 5°, the received signal falls off in amplitude and the individual "bits" become almost impossible to distinguish. This example shows only two "bits"; however, a longer string of similar "ones" and "zeros" would also suffer an analogous smearing as one moved away from the target position.

In this context, note that the *depth* of focus (i.e., the range of distance and angle over which the signal is comprehensible) depends strongly on the form and frequency content of the broadcast signal. For example, the waveform used in the experiment, which encompasses frequencies from 0.9 to 4.5 GHz (see Fig. 6), results in a received signal that distorts relatively quickly as the detector moves out beyond the target distance of $R_0 = 3.0$ m at the target angle (Fig. 10). By contrast, a relatively narrow-band broadcast signal (e.g., Fig. 3) will be recognizable at the target angle over a wider range of detector distances [24]. A full discussion of the criteria for the tightness of "information focusing" demands detailed analysis of many different broadband signal types and goes beyond the scope of the current work; instead, it forms the basis of a subsequent paper [27].

This technique represents a contrast to conventional radio transmission methods. In many instances of the latter, signals are broadcast with little or no directivity, selectivity of reception being achieved through the use of one or more narrow frequency bands [17,28–30]. In place of this, the current paper uses a spread of frequencies to transmit information to a particular location; the signal is weaker and has a scrambled time dependence elsewhere (Fig. 4). A possible application may be in proposed 5G neighborhood networks, where a single active antenna will sequentially spray bursts of information into a selection of target buildings around it [31,32]; ensuring that neighbors cannot easily understand what you are transmitting and receiving will be a useful component.

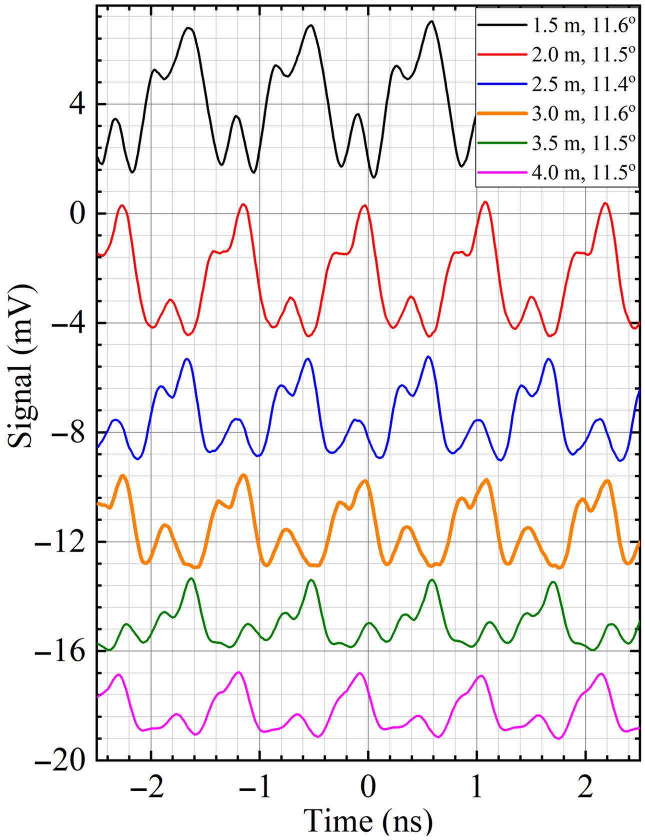

FIG. 10. Time dependence of the signal received by the detector dipole for azimuthal angle close to $\Phi_0 = 11.6^\circ$ and for different antenna-to-detector distances shown in the key. The shape of the transmitted waveform [Fig. 6(a)] is only reproduced close to the "target" $R_0 = 3.0$ m (orange trace).

The work in this paper may also be relevant to pulsars, rotating neutron stars that possess very large, off-axis magnetic fields and plasma atmospheres [33,34]. Pulsar periods of rotation $2\pi/\eta$ range from 1.5 ms to 8.5 s; a back-of-the-envelope calculation shows that at surprisingly small distances (85 km for the 1.5 ms pulsar; 40 000 km for the 8.5 s one) from the rotation axis, the pulsar's magnetic field will be traveling through its plasma atmosphere faster than the speed of light. Hydrodynamical models of pulsars [35–37] show the following: (i) electromagnetic disturbances (identifiable as polarization currents) exist outside the light cylinder, the orthogonal distance from the rotation axis r_L at which $\eta r_L = c$; (ii) these disturbances rotate at the same angular velocity as the neutron star's magnetic field (a requirement of Maxwell's equations), and so travel superluminally at radii outside the light cylinder; and (iii) the most intense disturbances are compact, in that they occupy a small fraction of the pulsar's atmosphere.

For such a compact source, traveling on a circular path at faster-than-light speeds, a derivation given in the Supplemental Material [21] shows that a plot of observation-detection time t_P versus emission time t exhibits "plateaux" (see Fig. 7 of the Supplemental Material) at, and only at, a special polar angle determined by the source's tangential speed. Apart from a single point at their center where $dt_P/dt = 0$, these "plateaux" are not, in fact, flat [24]. However, there is a reasonable region of t over which $dt_P/dt \ll 1$, so that a situation similar to that in Fig. 4(a) may be possible.

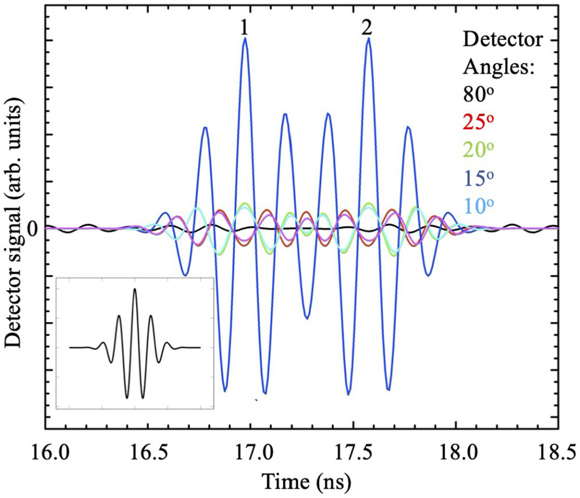

FIG. 11. Simulation of a notional method for transmitting information only to a target point. The inset shows a "bit" (consisting of a Gaussian convoluted with a cosine) as it would appear in the time dependence of the broadcast E field [compare with Fig. 3(c)]. The main figure shows a calculation of the detected signal at a range of 5 m. This results from time spacing two of these "bits" by three periods of the cosine function and then subjecting them to the same acceleration scheme that is used to produce Fig. 4. At the target angle of 15° (dark blue), the "bits" (labeled 1 and 2) may be easily resolved. However, as soon as the detector is moved to other angles (labeled by the colors in the key), the received signal is much weaker and the "bits" become virtually impossible to distinguish.

Pulsars can potentially emit electromagnetic radiation via many mechanisms [33,34], including thermal emission and other processes in their hot, plasma atmospheres, and dipole radiation from the rotating magnetic field of the neutron-star core; why then, might the pulsed radiation detected on Earth be dominated by the small volume of superluminal polarization current? The similarity of the "plateaux" in Fig. 7 of the Supplemental Material to Fig. 4(a) provides a useful clue. At the focus polar angle and over a short window of t_P, the frequency content of all of the emission processes occurring within the rotating polarization-current element will reproduce exactly, and result in a detected signal with greatly enhanced amplitude; the result is similar to coherent emission [38], but via a completely different mechanism. At all other observation angles and observation times, radiation from the emission processes will superpose incoherently [cf. Figs. 4(b) and 4(c)], leading to a greatly reduced amplitude, and scrambled frequency content. The sharp focusing in the time domain at the focus polar angle is likely to allow the radiation produced by the superluminal (outside the light cylinder) mechanisms to dominate the pulses. Note that this explanation of the brightness of pulsar pulses does not depend on the incorrect proposal [39] of nonspherical decay advocated by Ardavan [40–42].

VII. SUMMARY

The experiments in this paper show that a continuous, linear, dielectric antenna in which a superluminal polarization-current distribution accelerates can be used to transmit a broadband signal that is reproduced in a comprehensible form at a chosen target distance and angle. This is due to all of the radiation emitted from this point as it traverses the antenna reaching the observer-detector at the same time. For other observer-detector positions, the time dependence of the signal is scrambled, due to the nontrivial relationship between emission (retarded) time and reception time. The results may be relevant to 5G neighborhood networks and pulsar astronomy.

The data that support the findings of this study are available from the corresponding author upon reasonable request.

ACKNOWLEDGMENTS

The experiments and calculations in this paper are supported by Los Alamos National Laboratory LDRD Projects 20200285ER and 20180352ER. We are grateful for additional support from *LANL FY17 Pathfinder Fund Call for Technology Demonstration, PADGS:16-036*. Much of this work is performed at the National High Magnetic Field Laboratory, USA, which is supported by NSF Cooperative Agreements DMR-1157490 and DMR-1644779, the State of Florida and U.S. DoE. J.S. acknowledges a Visiting Professorship from the University of Oxford that enabled some of the calculations reported in this paper to be initiated. We thank Ward Patitz for his hospitality, assistance and very helpful suggestions during antenna prototyping experiments carried out at the FARM Range of Sandia National Laboratory. We are grateful for a former collaboration with H and A Ardavan [9,10] that gave the first hints of the potential of polarization-current antennas.

---

[1] A. Sommerfeld, Zur Elektronentheorie (3 Teile), Nach. Kgl. Ges. Wiss. Göttingen, Math. Naturwiss. Klasse, 99–130, 363–439 (1904), 201–35 (1905).

[2] G. A. Schott, *Electromagnetic Radiation and the Mechanical Reactions Arising from it* (Cambridge University Press, Cambridge, UK, 1912).

[3] V. L. Ginzburg, Vavilov-Čerenkov effect and anomalous Doppler effect in a medium in which wave phase velocity exceeds velocity of light in vacuum, Sov. Phys. JETP **35**, 1:92 (1972).

[4] B. M. Bolotovskii and A. V. Serov, Radiation of superluminal sources in vacuum, Radiat. Phys. Chem. **75**, 813 (2006).

[5] B. M. Bolotovskii and A. V. Serov, Radiation of superluminal sources in empty space, Phys. Usp. **48**, 903 (2005).

[6] A. V. Bessarab, A. A. Gorbunov, S. P. Martynenko, and N. A. Prudkoi, Faster-than-light EMP source initiated by short x-ray pulse of laser plasma, IEEE Trans. Plasma Sci. **32**, 1400 (2004).

[7] A. V. Bessarab, S. P. Martynenko, N. A. Prudkoi, A. V. Soldatov, and V. A. Terenkhin, Experimental study of electromagnetic radiation from a faster-than-light vacuum macroscopic source, Radiat. Phys.Chem. **75**, 825 (2006).

[8] Yu. N. Lazarev and P. V. Petrov, A high-gradient accelerator based on a faster-than-light radiation source, Tech. Phys. **45**, 971 (2000).

[9] A. Ardavan, W. Hayes, J. Singleton, H. Ardavan, J. Fopma, and D. Halliday, Corrected article: "Experimental observation of nonspherically-decaying radiation from a rotating superluminal source", J. Appl. Phys. **96**, 7760 (2004).

[10] J. Singleton, A. Ardavan, H. Ardavan, J. Fopma, D. Halliday, and W. Hayes, in *Conference Digest of the 2004 Joint 29th International Conference on Infrared and Millimeter Waves and 12th International Conference on Terahertz Electronics* (IEEE, Piscataway, NJ, USA, 2004), Cat. No. 04EX857.

[11] A. C. Schmidt-Zweifel, Master thesis, 2013, digitalrepository.unm.edu/math_etds/45/. Accessed January 2020.

[12] John Singleton, Houshang Ardavan, and Arzhang Ardavan, Apparatus and method for phase fronts based on superluminal polarization current, U.S. Patent No. 8,125,385 (February 2012).

[13] John Singleton, Lawrence M. Earley, Frank L. Krawczyk, James M. Potter, William P. Romero, and Zhi-Fu Wang, Superluminal antenna, U.S. Patent No. 9,948,011 (February 2012, reissued April 2018).

[14] Frank Krawczyk, John Singleton, and Andrea Caroline Schmidt, Continuous antenna arrays, U.S. Patent, filed August 2018 [USSN 62/721,031].

[15] John Singleton and Andrea Caroline Schmidt, Antenna and transceiver for transmitting a secure signal, U.S. Patent No. 9,722,724 (August 2017).

[16] J. D. Jackson, *Classical Electrodynamics* (John Wiley & Sons, Inc., New York, 1999), 3rd ed.

[17] C. A. Balanis, *Advanced Engineering Electromagnetics* (John Wiley & Sons, Inc., Hoboken, NY, 2012), 2nd ed.

[18] B. I. Bleaney and B. Bleaney, *Electricity and Magnetism*, The Oxford Classic Text Edition (Oxford University Press, Oxford, UK, 2013).

[19] O. D. Jefimenko, *Electricity and Magnetism: An Introduction to the Theory of Electric and Magnetic Fields* (Electret Scientific, Waynesburg, PA, 1989), 2nd ed.

[20] Philip Willmott, *An Introduction to Synchrotron Radiation: Techniques and Applications* (John Wiley and Sons, Chichester, 2019), 2nd ed.

[21] See Supplemental Material at http://link.aps.org/supplemental/10.1103/PhysRevApplied.14.064046 for additional experimental and theoretical details.

[22] Aldo Petosa, *Dielectric Resonator Antenna Handbook* (Artech House, Boston, 2007).

[23] Frank Krawczyk (to be published).

[24] A. C. Schmidt-Zweifel, Ph.D. thesis, University of New Mexico, 2020, available from digitalrepository.unm.edu.

[25] As mentioned above, the x and z extent of the antenna are small compared to its length. Therefore we ignore the slight variations in distance caused by the nonzero x depth and z height of the antenna and represent the motion of the volume-distributed polarization current by a function depending only on y and t.

[26] K. Nichols, J. Singleton, and A. C. Schmidt-Zweifel (to be published).

[27] A. C. Schmidt and J. Singleton (to be published).

[28] L. C. Godara (ed.), *Handbook of Antennas in Wireless Communications* (CRC Press, Boca Raton, 2002).

[29] David L. Adamy, *EW 103, Tactical Battlefield Communications – Electronic Warfare* (Artech House, Norwood, MA, 2009), 1st ed.

[30] Kenneth D. Johnston, *Analysis of Radio Frequency Interference Effects on a Modern Coarse Acquisition Code Global Positioning System Receiver* (Biblioscholar, New York, 2012).

[31] A. Nordrum and K. Clark, Everything You Need to Know About 5G, IEEE Spectrum (27 January, 2017) (https://spectrum.ieee.org – retrieved December 31, 2019).

[32] 5G Technology Introduction, https://telcomaglobal.com/blog/17780/5g-technology-introduction (retrieved February 01, 2020).

[33] D. R. Lorimer and M. Kramer, *Handbook of Pulsar Astronomy* (Cambridge University Press, Cambridge, UK, 2005).

[34] A. G. Lyne and F. Graham-Smith, *Pulsar Astronomy* (Cambridge University Press, Cambridge, UK, 2006).

[35] C. Kalapotharakos, I. Contopoulos, and D. Kazanas, The extended pulsar magnetosphere, Mon. Not. R. Astron. Soc. **420**, 2793 (2012).

[36] I. Contopoulos and C. Kalapotharakos, The pulsar synchrotron in 3D: Curvature radiation, Mon. Not. R. Astron. Soc. **404**, 767 (2010).

[37] A. Spitkovsky, Time-dependent force-free pulsar magnetospheres: Axisymmetric and oblique rotators, Astrophys. J. Lett. **648**, L51 (2006).

[38] G. A. Brooker, *Modern Classical Optics* (Oxford University Press, Oxford, 2003).

[39] A. Schmidt and J. Singleton, Flaws in the theory of electromagnetic radiation "whose decay violates the inverse-square law": Mathematical and physical considerations, *Plasma Phys.* (to be published).

[40] H. Ardavan, The mechanism of radiation in pulsars, Mon. Not. R. Astron. Soc. **268**, 361 (1994).

[41] H. Ardavan and J. E. Ffowcs Williams, Violation of the inverse square law by the emissions of supersonically or superluminally moving volume sources, arXiv:astro-ph/9506023v1 (1995).

[42] H. Ardavan, Generation of focused, nonspherically decaying pulses of electromagnetic radiation, Phys. Rev. E **58**, 6659 (1998).